KINETICS OF α-Fe NANOCRYSTALLIZATION IN $Fe_{55}Cr_{18}Mo_7B_{16}C_4$ BULK AMORPHOUS ALLOY

S. Ahmadi, H. R. Shahverdi* and S. S. Saremi

* shahverdi@modares.ac.ir

Faculty of Engineering, Department of Materials Science, Tarbiat Modares University, Tehran, Iran.

Abstract: *In this research work, crystallization kinetics of $Fe_{55}Cr_{18}Mo_7B_{16}C_4$ alloy was evaluated by X-ray diffraction, TEM observations and differential scanning calorimetric tests. In practice, crystallization and growth mechanisms were investigated using DSC tests in four different heating rates. Results showed that a two -step crystallization process occurred in the alloy in which α - Fe phase was crystallized in the first step after annealing treatments. Activation energy for the first step of crystallization i.e. α - Fe was measured to be 276 (kj/mol) according to Kissinger model. Further, avrami exponent calculated from DSC curves was 2 and a three -dimensional diffusion controlled mechanism with decreasing nucleation rate was observed in the alloy. It is also known from the TEM observations that crystalline á − Fe phase nucleated in the structure of the alloy in an average size of 10 nm and completely mottled morphology.*

1. INTRODUCTION

Bulk metallic glasses – BMGs – or bulk amorphous alloys have been attracted much attention during last decades due to their unique properties. A great number of efforts have been focused on Fe- base bulk amorphous alloys, as the new class of structural BAMs, due to their corrosion, magnetic, and mechanical properties. Crystallization from amorphous state and formation of nanosize crystals has been named as the most striking feature of the alloys. Indeed, unstable structures of bulk amorphous steels can be devitrified to stable nano structures composed of nanosize crystals and phases by controlled heat treatments above their crystallization temperatures [1-3].

It is true that there are a number of researches toward the characterization of crystallization kinetics in magnetic category of bulk amorphous steels but only a few attempts have been devoted about the detailed study of the crystallization behaviors of structural amorphous steels (SASs). In effect, crystallization kinetics of melt- spun $Fe_{83}B_{17}$ and $Fe_{75}Si_9B_{16}$ metallic glass has been investigated by A. A. Soliman et al. [4] and K. Chrissafis et al. [5] respectively using Johnson- Mehi- Avrami (JMA) model.

In case of the kinetic investigations non- isothermal analyses and related models i.e. Kissinger- Starink, Ozawa, Matusita, and Gao- Wang have been widely used to evaluate the kinetics of crystallization and devitrification in amorphous alloys [6]. In addition to activation energies of transformations, mechanisms of crystallization and growth (i.e. Avrami exponent, n) can be investigated in amorphous alloys using Matusita, and Gao-Wang models [7].

In this research, crystallization of nanosize α - Fe crystals in a Fe- B- Mo- Cr- C alloy during annealing process was investigated for the first time.

2. EXPERIMENTAL PROCEDURES

Fe- based amorphous alloy ingots were prepared in an arc furnace with nominal compositions of $Fe_{55}Cr_{18}Mo_7B_{16}C_4$ (an example of supper hard steels – SHS). Pure iron, chromium, molybdenum, and crystalline boron were utilized to produce ingots in a rod form. To achieve fully amorphous structures, rapidly solidified thin ribbons with a thickness of approximately 60 µm were prepared by melt-spinning technique (wheel speed: 32 m/s). Then, amorphous ribbons were annealed under vacuum (10^{-3} torr) in a furnace above the crystallization temperature. X- ray diffraction (XRD) with Cu Kα radiation and differential scanning calorimetric (DSC) test were used to determine the precipitated phases and transformation temperatures. A 200 kV JEOL transmission electron microscope equipped with an energy

S. Ahmadi, H. R. Shahverdi and S. S. Saremi

dispersive X-ray spectrometer (INCA PentaFETx3 - Oxford instruments) was used to microstructural evaluations.

3. RESULTS AND DISCUSSION

3. 1. Crystallization Kinetics

XRD pattern of $Fe_{55}Cr_{18}Mo_7B_{16}C_4$ alloy in amorphous state is shown In Figure 1. It can be seen clearly that there is no significant crystalline sharp peak in the chart indicating an amorphous structure.

Two peaks are observed in all thermograms showing two -stage crystallization process in the alloy. It is clear that the peak temperatures (T_{P1}, T_{P2}) increase with increasing the heating rate and this suggests that the crystallizations can be classified in the temperature dependent and diffusion controlled processes. In Table1 changes in the first (T_{P1}) crystallization peak with increasing heating rate are given.

In practice, annealing temperature was chosen above the first crystallization peak i.e. 650°C. Figure 2 shows the XRD pattern of crystallized ribbon annealed at temperature mentioned earlier.

It is clear from the Figures 2 that á - Fe phase

was crystallized in the structure after annealing process. In comparison with the pervious researches [4, 5], crystallization of $Fe_{23}C_6$ phase was not observed in the alloy; it is thought to be due to insufficient annealing time (3 hrs) in the alloy. Kissinger- Starink peak method (equation 1) [8] was used to investigate the activation energy, Ea, in the first step of crystallization. According to the equation 1, plotting $\ln(\beta/T_P^2)$ versus $1/T_P$ gives a straight line, the slope of it equals to -Ea/R [8].

$$\ln \frac{\beta}{T_P^2} = -\frac{E_a}{RT_P} + C \qquad (1)$$

Where β is heating rate, R is the gas constant, and T_p is the peak temperature.

Arrhenius plots for the first endothermic heat effect is shown in Figure 3. Activation energy for crystallization of $\alpha-$ Fe phase in the alloy was measured to be 276 (kj/mol) according to Kissinger model.

In comparison with other kinds of solid state transformations such as precipitation hardening, high value of activation energy in crystallization process of the amorphous alloy can be attributed to mass displacement of atoms. In other words,

Table 1. T_{P1} for four different heating rates.

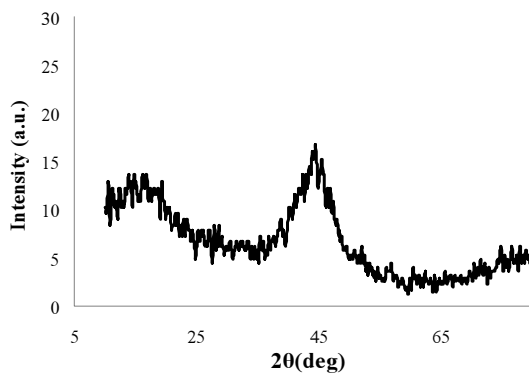| Heating Rate	10 K/min	20 K/min	30 K/min	40 K/min
T_{P1} (°C)	575	589	593	597

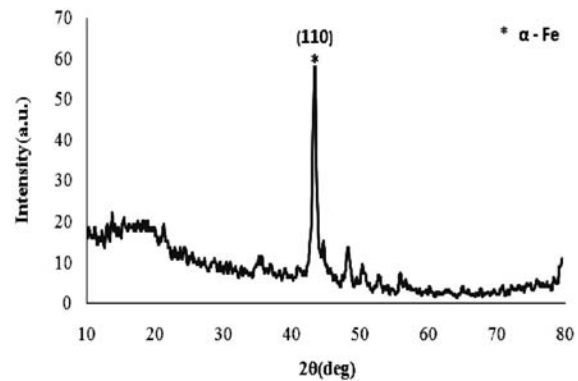**Fig. 1.** XRD pattern of the specimen in amorphous state.

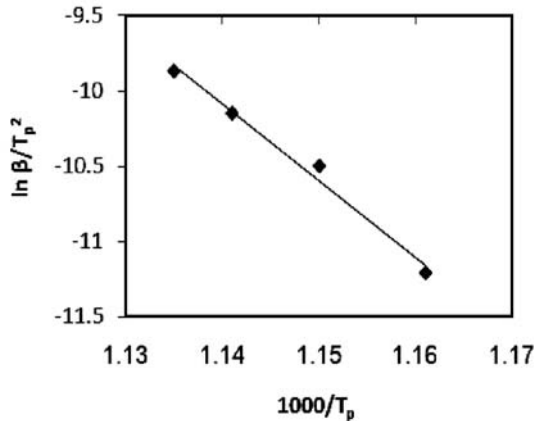**Fig. 2.** XRD pattern for specimen annealed at 650°C / 3 hrs.

Fig. 3. Arrhenius plot of $\ln(T_P^2/\beta)$ vs $1000/T_P$ for crystallization of α – Fe phase according to Kissinger model.

activation energy can be spent not only to overcome the energy barrier required to diffusion of atoms but also to nucleation and growth of crystalline phases. Specifically, activation energy in this research work was related to mass displacement of atoms in which α – Fe crystalline phase formed in the structure after annealing process. To indicate the exact mechanisms of growth in the alloy, Matusita model was used (equation 2).

$$ln\ [-ln(1-\alpha)]=-n\ ln\ (\beta)-1.052(mE_a/RT)+constant \qquad (2)$$

Where α is the volume fraction of crystallization, β is heating rate, E_a activation energy, n is Avrami exponent, m is dimensionality of growth, and R is the gas constant. In this
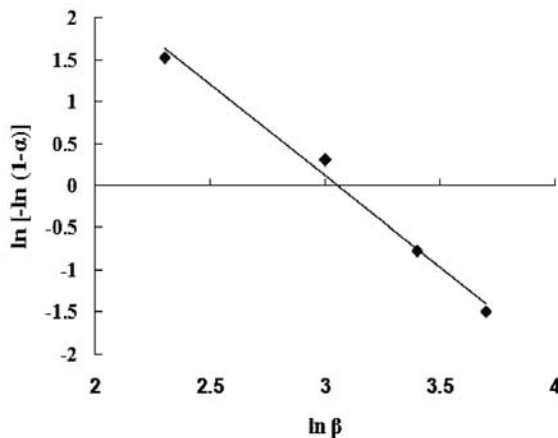
research, by plotting $\ln[-\ln(1-\alpha)]$ versus $\ln\beta$ at constant temperature Avrami exponent was estimated. Furthermore, by plotting $\ln[-\ln(1-\alpha)]$ versus temperature (T) at constant heating rate (β) dimensionality growth parameter (m) was derived. In Figures 4 and 5 variation of $\ln[-\ln(1-\alpha)]$ versus $\ln\beta$ at constant temperature and variation of $\ln[-\ln(1-\alpha)]$ versus temperature (T) at constant heating rate (β) are shown respectively.

Matusita model differs from Kissinger- Starink method in that it provides useful information about the Avrami exponent and dimension of growth in devitrification of amorphous alloys. Indeed, in addition to activation energy, mechanisms of growth can be investigated using this method. In general, Avrami exponent (n) can be estimated according to equation 3 [9].

$$n= b + pm \qquad (3)$$

Where n is Avrami exponent, m is dimensionality growth parameter, b is a parameter showing nucleation rate, and p is a parameter showing type of transformation e.g. diffusion controlled transformations. In Table 2 explanations of these parameters are given. The amount of Avrami exponent (n) in this research was calculated to be 2 by considering the slop of the straight line in Fig. 4.

In this research, the average of dimensionality growth parameter (m= 3) can be inferred from the slops of straight lines in Fig. 5. In fact, it is
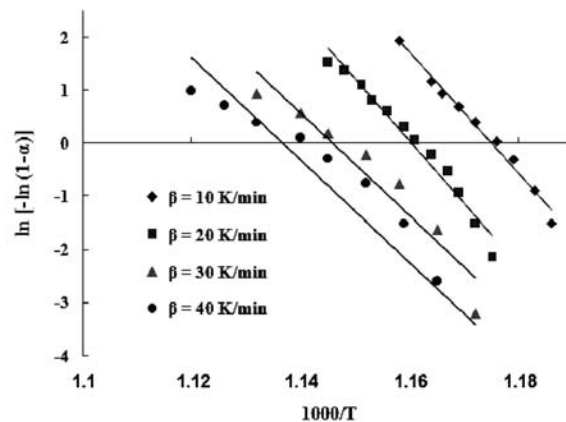

Fig. 4. Ln $[-\ln(1-\alpha)]$ as a function of heating rate in constant temperature (T=590°C).

Fig. 5. Matusita plots at different temperatures and constant heating rate.

though that devitrification process in $Fe_{55}Cr_{18}Mo_7B_{16}C_4$ was carried out by a bulk crystallization mechanism in three dimensions. By considering the growth parameters in Table 2, a diffusion controlled growth mechanism was accomplished in the alloy and thus, the amount of p was considered equal to 0.5. In addition, it is hypothesized that a decreasing nucleation rate (b) was also accomplished in crystallization of $Fe_{55}Cr_{18}Mo_7B_{16}C_4$ alloy resulted from equation 4 and the amounts of n, m, and p (2, 3, and 0.5 respectively).

3. 2. TEM Observations

In Fig. 6 microstructure of the primary alloy in amorphous state is shown. Specifically, no crystalline phases are detected in the figure. In Fig. 7 microstructure of the crystalline alloy after

heat treatment is shown. It is clear from the images that crystalline α – Fe in nucleate in the amorphous structure after annealing. Indeed, complex or partially crystalline structure formed due to heat treatment above the first crystalline temperature. Size and morphology of α –Fe crystalline phase are also indicated in Fig. 7. As can be seen clearly from the Figure, crystalline á – Fe phase nucleated in the structure an average size of 10 nm and completely mottled morphology.

4. CONCLUSIONS

1. A two- step crystallization process was observed in $Fe_{55}Cr_{18}Mo_7B_{16}C_4$ alloy in which α – Fe phase was crystallized in the first step of crystallization after annealing process.
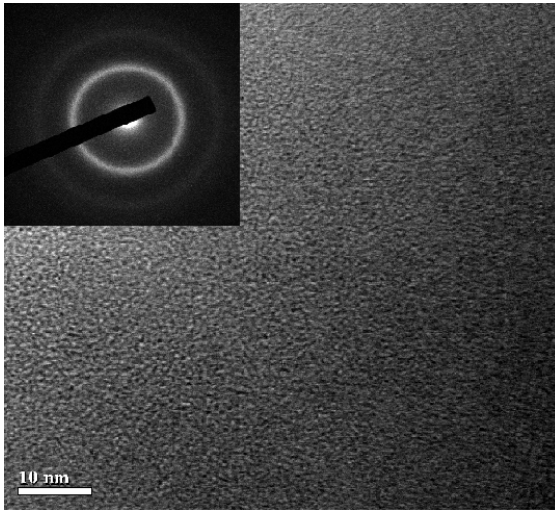

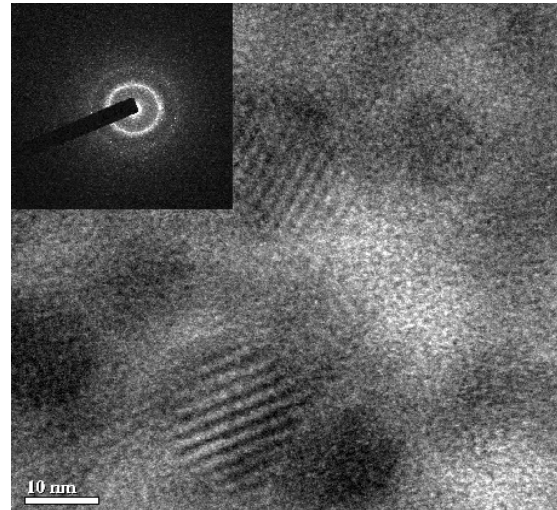**Fig. 6.** Microstructure of the alloy in amorphous state.

Fig. 7. Crystalline α –Fe phase into the amorphous structure.

Table 2. Explanation of nucleation and growth parameters [10, 11]

Parameter	Amount	Explanation
m	1	One- dimensional growth mechanism
	2	Two- dimensional growth mechanism
	3	Three- dimensional growth mechanism
p	1	Linear growth (interfacial control)
	0.5	Parabolic growth (diffusion control)
b	>1	Increasing nucleation rate
	0	No nucleation during crystallization (this means that all nuclei may be present before devitrification)
	<1	Decreasing nucleation rate

2. Activation energy for the crystallization of the phase α-Fe was measured to be 276 (kj/mol) according to Kissinger- Starink model.

3. Avrami exponent was measured to be 2 in the first step of crystallization of $Fe_{55}Cr_{18}Mo_7B_{16}C_4$ alloy.

4. A three -dimensional diffusion controlled growth mechanism and decreasing nucleation rate was found in crystallization of $Fe_{55}Cr_{18}Mo_7B_{16}C_4$ alloy.

5. Crystalline α–Fe phase nucleated in the structure of heat treated $Fe_{55}Cr_{18}Mo_7B_{16}C_4$ alloy in an average size of 10 nm and completely mottled morphology.

ACKNOWLEDGMENT

REFERENCES

1. Wang, W. H., Dong, C., Shek, C. H., Bulk Metallic Glasses, Mater. Science Eng. Reports, 2005, 44, 45.

2. Schroers, J., The superplastic forming of bulk metallic glasses, JOM, 2005, 57, 35-39.

3. Greer, A. L., Metallic Glass, Materialstoday, 2009, 12, 14.

4. Solima, A. A., Al-Heniti, S., Al-Hajry A., Al-Assiri M., Crystallization kinetics of melt-spun $Fe_{83}B_{17}$ metallic glass, Thermochim. Acta, 2004, 413, 57-62.

5. Chrissafi, K., Maragakis, M. I., Efthimiadis, K. G., Polychroniadis, E. K., Detailed study of the crystallization behaviour of the metallic glass $Fe_{75}Si_9B_{16}$, J. Alloys Compd., 2005, 386 165-173.

6. Minic, D. M., Maricic, A., Adnadevic, B., Crystallization of α-Fe phase in amorphous $Fe_{81}B_{13}Si_4C_2$ alloy, J. Alloys Compd., 2009, 473, 363-367.

7. Jain, R., Saxena, N. S., Bhandari, D., Sharma, S. K., Crystallization kinetics of CuxTi100x (x=43, 50 and 53) glasses, Physica B, 2001, 301, 341-345.

8. Starink, M. J., Analysis of aluminium based alloys by calorimetry: quantitative analysis of reactions and reaction kinetics, J. Int. Mater. Rev., 2004, 49, 191-226.

9. Ahmadi, S., Arabi, H., Shokuhfar, A., Formation mechanisms of precipitates in an Al–Cu–Li–Zr alloy and their effects on strength and electrical resistance of the alloy, J. Alloys Compd., 2009, 484, 90–94.

10. Farmer, J. C., and et al, HIGH-PERFORMANCE CORROSIONRESISTANT MATERIALS: IRON-BASED AMORPHOUS-METAL THERMAL-SPRAY COATINGS SAM, UCRL-TR-234787 SAM HPCRM program, FY04 annual report, 2004.

11. Pratap, A., Lad, K., Majmudar, T. Rao. P., Saxena, N. S., Estimation of Gibbs free energy difference in bulk metallic glass forming alloys J. Non- Crys. Solids, 2004, 345 & 346, 178-181.